Conformational Flexibility of PEP Mutase[†,‡]

Sijiu Liu,[§] Zhibing Lu,[∥] Ying Han,[∥] Yong Jia,[∥] Andrew Howard,[⊥,@] Debra Dunaway-Mariano,[∥] and Osnat Herzberg*[,§]

Center for Advanced Research in Biotechnology, University of Maryland Biotechnology Institute, 9600 Gudelsky Drive, Rockville, Maryland 20850, Department of Chemistry, University of New Mexico, Albuquerque, New Mexico 87131, Advanced Photon Source, Argonne National Laboratory, Argonne, Illinois 60439, and Biological, Chemical, and Physical Science Department, Illinois Institute of Technology, Chicago, Illinois 60616-3793

Received December 16, 2003; Revised Manuscript Received February 7, 2004

ABSTRACT: Previous work has indicated that PEP mutase catalyzes the rearrangement of phosphoenolpyruvate to phosphonopyruvate by a dissociative mechanism. The crystal structure of the mutase with Mg(II) and sulfopyruvate (a phosphonopyruvate analogue) bound showed that the substrate is anchored to the active site by the Mg(II), and shielded from solvent by a large loop (residues 115−133). Here, the crystal structures of wild-type and D58A mutases, in the apo state and in complex with Mg(II), are reported. In both unbound and Mg(II)-bound states, the active site is accessible to the solvent. The loop (residues 115−133), which in the enzyme−inhibitor complexes covers the active site cavity, is partially disordered or adopts a conformation that allows access to the cavity. In the apo state, the residues associated with Mg(II) binding are poised to accept the metal ion. When Mg(II) binds, the coordination is the same as that previously observed in the enzyme−Mg(II) sulfopyruvate complex, except that the coordination positions occupied by two ligand oxygen atoms are occupied by two water molecules. When the loop opens, three key active site residues are displaced from the active site, Lys120, Asn122, and Leu124. Lys120 mediates Mg(II) coordination. Asn122 and Leu124 surround the transferring phosphoryl group, and thus prevent substrate hydrolysis. Amino acid replacement of any one of these three loop residues results in a significant loss of catalytic activity. It is hypothesized that the loop serves to gate the mutase active site, interconverting between an open conformation that allows substrate binding and product release and a closed conformation that separates the reaction site from the solvent during catalysis.

Conversion of phosphoenolpyruvate (PEP)[1] to phosphonopyruvate (P-pyr) is catalyzed by PEP mutase, a 38 kDa tetrameric Mg(II)-dependent enzyme (*1*, *2*):

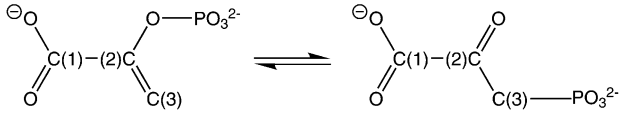

This P−C bond forming reaction serves as the point of entry to all known phosphonate biosynthetic pathways (*3*). The crystal structure of the PEP mutase from the mollusk *Mytilus edulis* was determined in the presence of Mg(II) oxalate, a tight binding Mg(II) pyruvate enolate homologue (*4*), revealing a tetrameric structure in which each molecule adopts an α/β barrel fold, with pairwise swapping of the eighth helix. To further investigate the catalytic mechanism, a second structure of the enzyme was determined, that in complex with the inhibitor sulfopyruvate (S-pyr), a compound isosteric with P-pyr with the sulfur replacing phosphorus. That structure, in conjunction with a site-directed mutagenesis probe of potential catalytic residues, suggested that catalysis proceeds via a dissociative mechanism involving the intermediacy of metaphosphate and the enolate anion of pyruvate (*5*). Both Mg(II) oxalate and Mg(II) S-pyr bind in the same location, at the center of the barrel, close to the C-terminal ends of the β-strands, and in both cases, two loop regions and part of the kinked C-terminal helix of the neighboring molecule bury the inhibitors and prevent access to the active site. We speculated that desolvation of the substrate may be required to prevent hydrolysis of the metaphosphate intermediate. Thus, substrate binding and dissociation must be accompanied by conformational changes (*4*, *5*).

The two loops that block access to the active site also contribute catalytic groups to the active site (*5*). The first loop comprises residues 47−62, and the key amino acid on this segment is Asp58. Replacement of Asp58 with a serine or alanine inactivates the enzyme, and replacement with asparagine preserves 0.05% of the original activity. In addition, residues 47−52 form a short helix whose N-terminus interacts with the carboxyl moiety of the inhibitor. The second loop comprises residues 115−133 (115−133

[†] Supported by NSF Grant MCB9813271 (O.H.) and NIH Grant GM36260 (D.D.-M.).

[‡] The coordinates have been deposited in the Protein Data Bank (entry codes 1S2T, 1S2U, 1S2V and 1S2W).

* To whom correspondence should be addressed. Telephone: (301) 738-6245. Fax: (301) 738-6255. E-mail: osnat@carb.nist.gov.

[§] University of Maryland Biotechnology Institute.

[∥] University of New Mexico.

[⊥] Argonne National Laboratory.

[@] Illinois Institute of Technology.

[1] Abbreviations: PEP, phosphoenolpyruvate; P-pyr, phosphonopyruvate; S-pyr, sulfopyruvate; PEP mutase, phosphoenolpyruvate mutase; HEPES, *N*-(2-hydroxyethyl)piperazine-*N*′-ethanesulfonic acid.

10.1021/bi036255h CCC: $27.50
Published on Web 03/25/2004

Table 1: Crystallization Conditions

crystal form	protein sample	reservoir solution	temp (°C)	flash-cooling solution
I	15 mg/mL wild-type (wt) protein, 20 mM HEPES buffer (pH 7.5)	18% PEG 4K, 0.1 M Tris-HCl buffer (pH 7.0−8.0)	25	15% PEG 4K, 20% glycerol, 0.1 M Tris-HCl (pH 7.5)
II	10 mg/mL D58A mutant, 5 mM $MgCl_2$, 5 mM P-pyr, 20 mM HEPES buffer (pH 7.5)	18% PEG 4K, 20% glycerol, 0.1 M HEPES buffer (pH 7.0−8.0)	25	like crystallization conditions
III	9 mg/mL wt protein, 5 mM $MgCl_2$, 20 mM triethanolamine buffer (pH 7.5)	18% PEG 4K, 15% glycerol, 0.1 M HEPES buffer (pH 7.0−8.0)	25	like crystallization conditions
IV	9 mg/mL wt protein, 5 mM $MgCl_2$, 20 mM triethanolamine buffer (pH 7.5)	40−44% saturated $(NH_4)_2SO_4$, 0.1 M HEPES buffer (pH 7.0)	37	90% saturated $Li_2(SO_4)$, 0.1 M HEPES (pH 7.0)

Table 2: Data Processing Statistics

	crystal I	crystal II	crystal III	crystal IV
space group	$C222_1$	$C222_1$	$P2_12_12$	$C222_1$
unit cell dimensions (Å)				
a	110.77	108.54	122.39	76.63
b	120.88	119.75	86.41	116.56
c	88.99	88.38	103.97	72.82
no. of molecules in the asymmetric unit	2	2	4	1
resolution range (Å)	39.1−1.99	27.7−2.0	38.0−2.1	29.3−1.69
last shell	2.06−1.99	2.05−2.00	2.18−2.10	1.75−1.69
no. of unique reflections [$F > 1\sigma(F)$]	40649	36902	62612	35608
redundancy	6.79	5.48	5.99	6.47
completeness (%)[a]	98.2 (85.4)	94.1 (84.5)	96.2 (91.1)	96.5 (86.8)
R_{merge}[a,b]	0.043 (0.136)	0.061 (0.299)	0.069 (0.238)	0.043 (0.259)
$\langle I/\sigma(I)\rangle$	20.0	10.4	9.1	12.3

[a] The values in parentheses are for the highest-resolution shell. [b] $R_{merge} = \sum_{hkl}[(\sum_j|I_j - \langle I\rangle|)/\sum_j|I_j|]$ for equivalent observations.

loop). Here, Lys120 plays a role by modulating the electrostatic interactions between Mg(II) and its coordinating ligands. Asn122 forms an electrostatic interaction with the sulfo oxygen of the sulfopyruvate ligand, and is thus implicated in substrate binding. The N122A mutant retains only 0.02% of the activity of the wild-type mutase. A third structural unit is involved in inhibitor desolvation, residues 271−280 of the kinked C-terminus helix of a neighboring molecule that traverses the top of the active site.

For a substrate to diffuse into the active site, one or more of the above structural units must be mobile. We report here four crystal structures of PEP mutase, three of the wild-type enzyme and one of the mutant D58A that reveal modes of conformational flexibility of the enzyme. The importance of loop (residues 115−133) closure over the active site is confirmed by site-directed mutagenesis studies of loop residues Lys120 and Leu124.

MATERIALS AND METHODS

Crystallization and X-ray Data Collection. The recombinant protein was prepared as described previously (*6*). Since the enzyme sample was obtained in a solution containing 5 mM $MgCl_2$, the Mg(II)-free sample was prepared by repetitive dilution and concentration steps using 20 mM HEPES buffer (pH 7.5) prepared with distilled and deionized water to produce a final 1.6×10^8-fold dilution (i.e., 30 pM $MgCl_2$). At this concentration, the enzyme is expected to be predominantly at the apo state because Mg(II) binds to PEP mutase with a K_d of 0.3 mM (*7*). Indeed, the corresponding crystal structure shows no evidence of bound Mg(II). Crystals were obtained by vapor diffusion in hanging drops. Four different crystals were prepared, three under low-ionic strength conditions (denoted crystal forms I−III) and one at high ionic strength (crystal form IV). Protein drops mixed with equal volumes of reservoir solutions were equilibrated at room temperature or 37 °C against the respective reservoir solutions. Table 1 provides the crystallization conditions.

For X-ray data collection, crystals were transferred to appropriate cryogenic solutions (Table 1) and flash-cooled in liquid propane cooled with liquid nitrogen. Diffraction data were collected at 100 K on the IMCA-CAT 17-BM beamline equipped with a MAR CCD detector at the Advanced Photon Source. Data were processed with HKL (*8*). Statistics of data collection are provided in Table 2.

Structure Determination and Refinement. The crystal forms reported here were different from those of the two previously determined structures. Each of the new structures was determined by molecular replacement using AmoRe (*9*). The search model was that of the structure of the enzyme−Mg(II) oxalate complex (PDB entry 1pym), omitting the Mg(II) oxalate and solvent molecules. Difference Fourier maps were calculated, and segments of the polypeptide chain that could not be traced in the electron density were omitted from the model. In some cases, alternative tracing was evident, and new interpretations were possible. In other cases, there was no electron density to account for the omitted polypeptide, indicating disorder. The structures were refined with CNS (*10*), first using simulated annealing at 3000 K, and then alternating positional and individual temperature factor refinement cycles. Individual molecules in the asymmetric units were refined independently. The progress of the refinement was evaluated by the improvement in the quality of the electron density maps, and the reduced values of the conventional *R* factor ($R = \sum_h||F_o| - |F_c||/\sum_h|F_o|$, where F_o and F_c are the observed and calculated structure factors, respectively) and R_{free} (7−9% of the reflections omitted from

Table 3: Refinement Statistics

	crystal I	crystal II	crystal III	crystal IV
resolution range (Å)	39.1−1.99	27.7−2.0	38.0−2.1	29.3−1.69
no. of unique reflections [$F > 2\sigma(F)$]	39056	33155	52982	32538
completeness (%)	94.6	84.6	81.3	88.2
R_{work}[a]	0.168	0.165	0.184	0.178
R_{free}[a]	0.216	0.219	0.254	0.207
rmsd from ideal geometry				
bond lengths (Å)	0.010	0.008	0.012	0.009
bond angles (deg)	1.5	1.4	1.5	1.4
average *B* factor (Å^2)				
protein	23	22	34	24
Mg(II)	−	−	39	−
H_2O	36	32	42	39

[a] $R_{work} = \sum_{hkl}||F_o| - |F_c||/\sum_{hkl}|F_o|$, where F_o and F_c are the observed and calculated structure factors, respectively. R_{free} is calculated for randomly selected reflections that were omitted from the refinement. These were 7.6, 8.5, 6.6, and 8.8% of the reflections for crystals I−IV, respectively.

the refinement) (*11*). Difference Fourier electron density maps were inspected, and the models were modified on an interactive graphics workstation with O (*12*). Water molecules and other solvent entities were added gradually as the refinement progressed. They were assigned in the $|F_o| - |F_c|$ difference Fourier maps with a 3σ cutoff level for inclusion in the model.

Site-Directed Mutants. Site-directed mutagenesis was carried out using a PCR-based strategy with the YJ102 clone as described previously (*6*). Mutant plasmids isolated from JM109 *Escherichia coli* host cells were subjected to DNA sequencing to verify the correct PEP mutase gene sequence, and then used to transform BL21(BE3) *E. coli* cells for expression. The PEP mutase mutants were purified to homogeneity (as judged by SDS−PAGE analysis) using the same method that was used to purify wild-type recombinant PEP mutase.

Steady-State Kinetic Measurements. The k_{cat} and K_m values for wild-type and mutant PEP mutase were determined from initial velocity data. The rate of PEP formation in reactions including PEP mutase, 5 mM $MgCl_2$, varying concentrations of P-pyr (prepared according to the method of ref *13*) (1−10-fold K_m), 50 mM K^+HEPES (pH 7.5 and 25 °C), and the coupling system (1 mM ADP, 0.2 mM NADH, 10 units/mL pyruvate kinase, and 10 units/mL lactate dehydrogenase) was monitored by measuring the decrease in solution absorbance at 340 nm ($\Delta\epsilon = 6.2$ mM^{-1} cm^{-1}). The initial velocity data were analyzed using eq 1 and the computer program of Cleland (*14*):

$$v_0 = V_m[S]/(K_m + [S]) \quad (1)$$

where v_0 is the initial velocity, V_{max} is the maximum velocity, [S] is the substrate concentration, and K_m is the Michaelis constant for the substrate. The k_{cat} values were calculated from V_m and the enzyme concentration, [E], according to the equation $k_{cat} = V_{max}/[E]$. The protein concentration was determined using the Bradford assay (*15*).

RESULTS AND DISCUSSION

Overall Structure. Statistics of the structure refinements are provided in Table 3. The four reported models are as follows.

(a) Apo PEP mutase (crystal I) includes residues 5−124 and 126−295 of one molecule (i.e., no electron density is associated with residue 125) and residues 4−123, 126, and 128−294 of the second molecule in the asymmetric unit. In addition, the model includes 639 water molecules. The root-mean-square deviation (rmsd) between α-carbon atom positions of the two molecules is 0.2 Å. The molecules pack into tetramers with 222 symmetry, using both the noncrystallographic and crystallographic 2-fold symmetry axes. Residues 117−132 of each molecule of the asymmetric unit adopt a new conformation compared with that of the Mg(II) oxalate- and Mg(II) S-pyr-bound protein structures. The new loop conformation results in a solvent accessible active site. Otherwise, the rmsd between α-carbon atom positions of apo-PEP mutase and each of the earlier Mg(II) oxalate and Mg(II) sulfopyruvate structures, excluding loop residues 115−133, varies between 0.3 and 0.4 Å.

(b) The model with D58A PEP mutase with Mg(II), and P-pyr (crystal II) includes residues 5−295 of one molecule and residues 5−123 and 128−293 of the second molecule in the asymmetric unit. Mg(II) ions or P-pyr could not be identified in the electron density map. Instead, there is density in each active site, consistent with binding of dihydroxyethyl ether, which probably originated from the PEG 4000 solution used for crystallization. In addition, the model includes 567 water molecules.

The rmsd between α-carbon atom positions of the two protein molecules of the asymmetric unit is 0.2 Å. This is essentially the same crystal form as that of apo-PEP mutase crystal I, with the same loop conformation of residues 117−132 (except for variation in the identity and extent of disordered residues in the loop). The rmsd between α-carbon atom positions of D58A PEP mutase and apo-PEP mutase is 0.3 Å.

(c) The PEP mutase−Mg(II) low-ionic strength structure (crystal III) contains four molecules in the asymmetric unit and includes residues 5−122 and 130−293 of one molecule, residues 4−123 and 128−293 of the second molecule, residues 4−120 and 130−293 of the third molecule, and residues 4−119 and 130−293 of the fourth molecule. Hence, segments of the 115−133 loop in each molecule are disordered to different extents. The four molecules of the asymmetric unit pack into two dimeric subassemblies, each belonging to a different tetramer, and the complete tetramers are generated by crystallographic symmetry axes. Mg(II) ions were assigned in each of the four active sites. The electron density map for one of these sites is shown in Figure 1. The

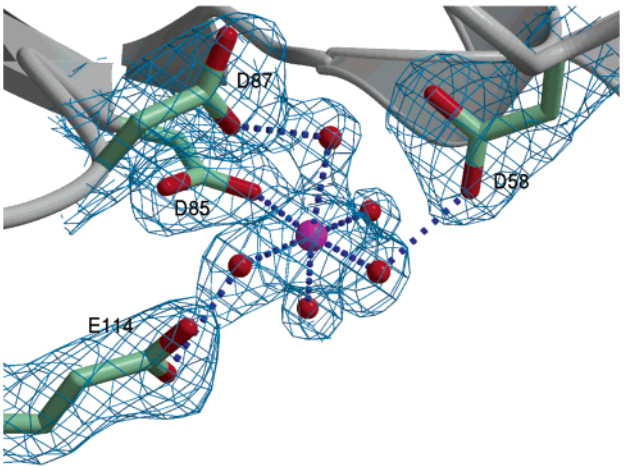

FIGURE 1: Electron density map surrounding the Mg(II) in crystal structure III together with the final model. A difference Fourier map with the $2F_o - F_c$ coefficients and calculated phases is shown. The map is contoured at 1σ. Mg(II) is shown as a magenta sphere. Key carboxylate-containing residues are shown as stick models with atomic coloring (pale green for carbon and red for oxygen). Water molecules are shown as red spheres. Electrostatic interactions are represented as dashed lines.

crystallographic temperature factors of the Mg(II) and associated water molecules are high (Table 3), perhaps because the site is not fully occupied. The model includes 944 water molecules.

The rmsd between α-carbon atom positions of any pair of molecules in the asymmetric unit is 0.3 Å. The rmsd between α-carbon atom positions of molecule A or B of the asymmetric unit and the molecules of the apoprotein in crystal I, excluding residues 115−133, is 0.2 Å, and the corresponding rmsd for molecule C or D is 0.3 Å. The rmsd between α-carbon atom positions of crystal III molecules and the Mg(II) oxalate- or Mg(II) sulfopyruvate-bound structures, excluding residues 115−133, varies between 0.3 and 0.4 Å.

(d) The PEP mutase−Mg(II) high-ionic strength structure (crystal IV) assembles into dimers rather than tetramers. The dimers are generated by the crystallographic symmetry. Despite the high resolution of the data (1.7 Å), the molecule exhibits more disorder than the three crystal structures obtained at low ionic strengths. Electron density is missing for residues 1−3, 55−63, 117−126, and 279−295, and the main chain of active site Gly46 adopts a β conformation instead of the helical conformation seen in all other structures. No electron density corresponding to Mg(II) is present in the active site, perhaps because of the high ionic strength of the crystallization solution. Density that fits the shape of an aspartic acid or asparagines is present in the active site. The hypothesis that such a ligand may have originated from degradation of the protein sample was dismissed on the basis of the experimental finding that the enzyme is not inhibited by either of these amino acids. For lack of a better ligand, a sulfate ion was included with half an occupancy. In addition, the model includes 270 water molecules.

Loop Opening and Active Site Access. The four structures reported here belong to three different crystal forms. All exhibit active sites that are accessible to solvent, and thus correspond to enzyme states when substrate and product can diffuse in and out. Crystal forms I−III were obtained from low-ionic strength solutions, and active site access is observed because of changes to the 115−133 loop. For the high-ionic strength crystal form IV, two more regions exhibit disorder (i.e., the Asp58-containing segment and the C-terminus), but in addition, the enzyme assembles into dimers rather than tetramers. The dimeric subassembly is facilitated by hydrophobic interactions due to the swapped helices. The association of dimers into a tetramer is mediated by a mixture of hydrophilic and hydrophobic interactions. This mode of association has been eliminated, presumably because the high concentration of ammonium sulfate screens the electrostatic interactions.

From a structural point of view, the dimer association seen in the high-salt crystal contains all the necessary features for enzymatic activity (i.e., the C-terminal segment of one molecule that participates in blocking solvent access to the active site of the neighboring molecule is present, and is structurally ordered), yet it is not known whether a dimeric subassembly is a functional form of the enzyme. Moreover, the high-salt crystal form may be physiologically irrelevant because the substrate and product are highly charged and high ionic strength may reduce their binding affinity. We therefore propose that the structures determined at low ionic strengths better represent the native structure, and that they indicate the primary conformational transition responsible for enzyme activity is that involving the 115−133 loop.

A superposition of the apo-PEP mutase structure (molecule A) on that of the enzyme−Mg(II) S-pyr complex highlights the similarity between the overall fold and the striking difference between the open and closed conformations of the 115−133 loop (Figure 2a). For the second low-ionic strength crystal form (crystal III), a large segment of the loop is disordered, which also leads to an accessible active site. Mg(II) is present in crystal III, but the "lid" is still open, to enable the substrate to diffuse into the active site.

One of the possible determinants of loop conformation is Lys120. When the loop closes, the positively charged amino group of Lys120 is located in the vicinity of the Mg(II) (3.8 Å). The charge groups in the active site are exquisitely arranged. In addition to Mg(II) and Lys120, the site contains Arg159, the highly negatively charged substrate, and several carboxylate groups that coordinate or mediate water coordination to Mg(II). This charge balance favors loop closure in the presence of the negatively charged substrate. Prior to substrate binding, the proximity of Mg(II), Lys120, and Arg159 is energetically unfavorable. Arg159 is located on one of the barrel β-strands and cannot move without a gross disruption of the overall fold. In contrast, a conformational transition of the 115−133 loop is possible, and the opening moves the amino group of Lys120 11 Å from its position at the bound state (Figure 2b). Consistent with the proposed regulatory role of Lys120, site-directed mutagenesis data reported in Table 4 show that Lys120 is important for catalytic activity. The k_{cat}/K_m of the K120R mutant (Arg substitution conserves the charge and steric bulk of the side chain but alters the orientation of the charged group) is reduced 420-fold from that of wild-type mutase, while the k_{cat}/K_m of the K120A mutant (charge and steric bulk of side chain removed) is reduced 2840-fold.

The Mg(II) in structure III is located in the same position as in the two previously reported enzyme−inhibitor complexes (Figure 3). Mg(II) binds directly to the carboxylate

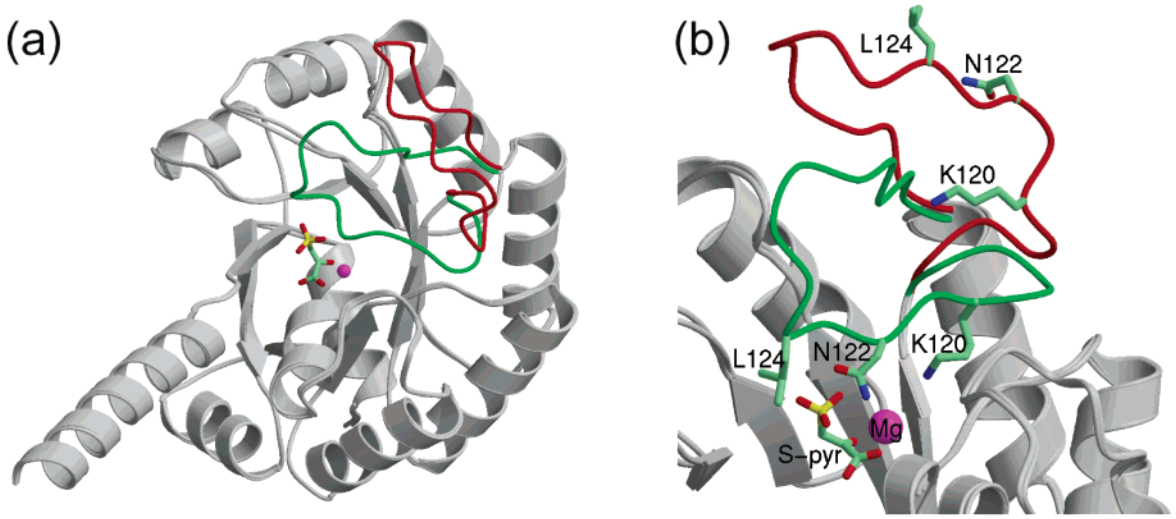

FIGURE 2: Superposition of the apo-PEP mutase monomer on that of the enzyme bound to Mg(II) S-pyr, an enzyme product analogue. Most of the structure has not changed, and for clarity is shown in gray for both molecules. The 115−133 loop is shown in red for the apoenzyme and in green for the inhibitor-bound complex. S-pyr and protein residues are shown as a stick model (atomic colors are used, pale green for carbon, red for oxygen, blue for nitrogen, and yellow for sulfur), and Mg(II) as a magenta sphere: (a) overall view and (b) close-up of the loop region, and depicting the key residues (K120, N122, and L124). In the apoenzyme structure, these residues are exposed to solvent because of the conformation transition of the 115−133 loop.

Table 4: Steady-State Kinetic Constants Determined for Wild-Type and Mutant PEP Mutase[a]

PEP mutase	k_{cat} (s^{-1})	K_m (μM)	k_{cat}/K_m (s^{-1} M^{-1})
wild-type	3.4×10	1.6 ± 0.1	2.1×10^7
K120A	3.4×10^{-1}	46 ± 2	7.4×10^3
K120R	3.2×10^{-1}	5.9 ± 0.4	5.4×10^4
L124A	9.8×10^{-3}	60 ± 3	1.6×10^2
N122A[b]	6.0×10^{-3}	38 ± 1	1.6×10^2

[a] Reaction mixtures contained varying concentrations of P-pyr (1−10-fold K_m), 5 mM $MgCl_2$, 50 mM K^+HEPES (pH 7.5 and 25 °C), and the coupling system (1 mM ADP, 0.2 mM NADH, 10 units/mL pyruvate kinase, and 10 units/mL lactate dehydrogenase). [b] Values from ref *5*.

group Asp85, and to five water molecules. The Mg(II) in molecule D exhibits the best geometry, forming octahedral coordination with average metal−ligand distance of 2.2 Å. The three remaining molecules also bind Mg(II), but the geometry is distorted probably because of the limited resolution of the diffraction data. Of the five coordinating water molecules, three interact with the carboxylate groups of Asp87, Asp58, and Glu114, as seen in inhibitor-bound enzyme structures. The two remaining water molecules bind in the same positions as the two oxygen atoms of the inhibitors in the enzyme−inhibitor complexes (*4*, *5*). Thus, all enzyme components except for the 115−133 loop are poised to bind substrate.

The sulfo group in the enzyme−Mg(II) S-pyr complex is located close to the side chains of Asn122 and Leu124. These residues are solvent-exposed in the open conformation (Figure 2b). Unlike the Mg(II)-bound enzyme structure (structure III), the apoenzyme structure (structures I) reveals most of the segment of residues 120−129, showing that Asn122 and Leu124 are remote from the active site (although their crystallographic temperature factors are high, and in molecule B the side chains of Asn122 and the entire Leu124 are disordered). The positions of the α-carbon atoms of Asn122 and Leu124 are approximately 16 and 18 Å from their positions in the closed conformation, respectively. In the enzyme−S-pyr complex, the side chains of Asn122 and Leu124 shield the sulfo group from solvent, and thus, we hypothesize that with a true substrate these side chains protect the metaphosphate intermediate from solvent capture. Table 4 shows that replacement of Asn122 or Leu124 with Ala results in a 1×10^5-fold decrease in the k_{cat}/K_m. The significant loss of catalytic activity suggests that these residues may contribute to the stabilization of the closed loop conformation wherein Asn122 interacts with Asp58 and Leu124 is desolvated.

Role of Asp58. Asp58 is essential for enzyme activity, yet the structure of the enzyme−Mg(II) S-pyr complex shows that Asp58 is remote from the sulfo group of S-pyr, ruling out our earlier proposal that the side chain of Asp58 functions as a phosphoryl group acceptor in a phosphotransfer reaction that proceeds via an associative mechanism (*5*). In the two inhibitor−enzyme complexes, the carboxylate group of Asp58 interacts with one of the Mg(II) coordinating water molecules, and with Asn122. That water molecule also interacts with the amino group of Lys120 and with the amide group of Asn122 (Figure 3b). We proposed that the interactions of Asn122 with Asp58 and with the Mg(II)-coordinating water molecule are critical for activity because they regulate loop closure.

The D58A mutant exhibits no detectable enzymatic activity. Therefore, this mutant enzyme seemed to be a suitable candidate for obtaining crystals of a protein−substrate or protein−product complex, yet cocrystallization of the mutant enzyme and Mg(II) P-pyr yielded essentially the same crystals and the same structure as the apoprotein, with an open loop conformation and no bound Mg(II). Note that the crystallization solutions of the various structures are quite similar, indicating that the failure to trap the D58A PEP mutase in a bound state is an inherent property of the mutant protein, and not of the crystallization conditions. Because the only change compared with the wild-type protein is the elimination of the aspartic acid side chain at position 58, we may conclude that the Asp58−Asn122−Lys120

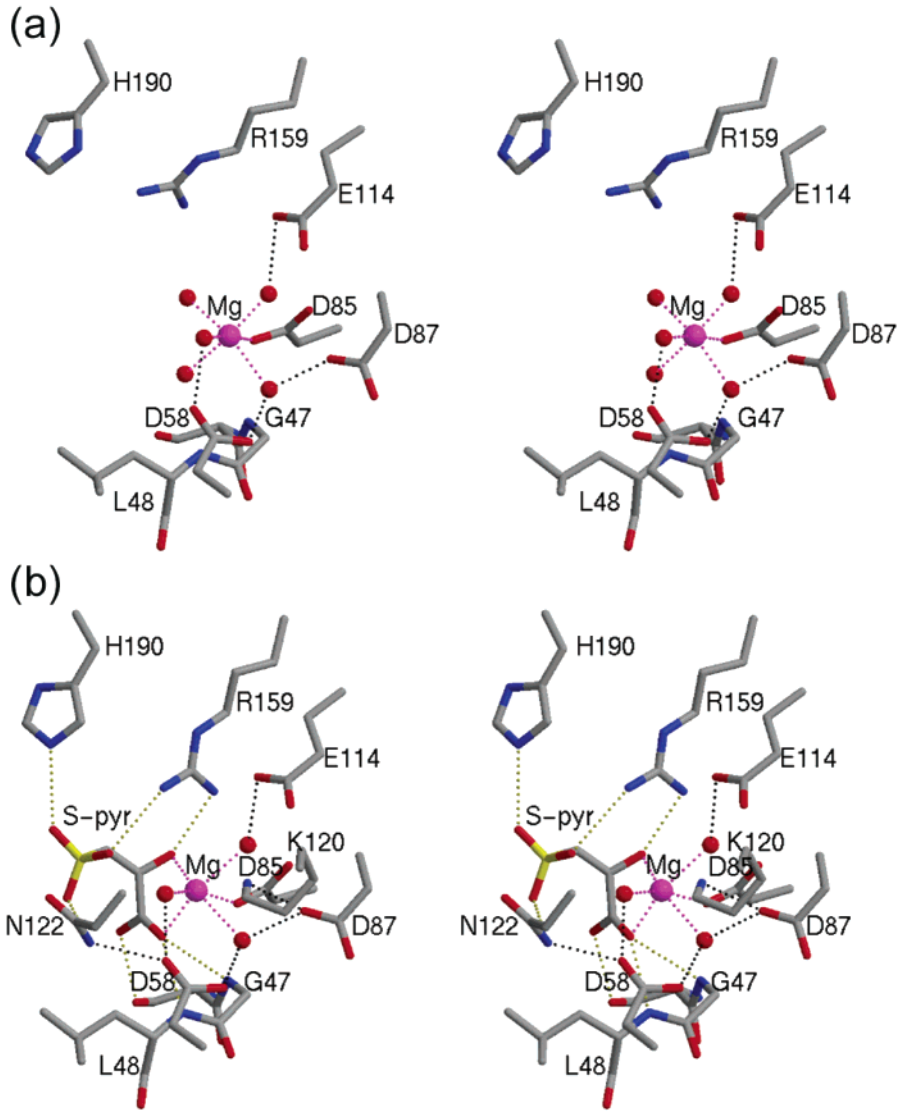

FIGURE 3: Stereoscopic representation of active site interactions. Atomic colors are as follows: red for oxygen, gray for carbon, yellow for sulfur, and magenta for Mg^{2+}: (a) Mg(II)-bound enzyme (open conformation) and (b) Mg(II) S-pyr complex. Key interactions are highlighted with dotted lines as follows. Coordination to the Mg(II) is shown in magenta; electrostatic interactions with S-pyr are shown in yellow, and protein interactions with Mg(II)-coordinated water molecules are shown in gray.

interaction is essential for loop closure, without which the enzyme is inactive. Asp58 may also be important for Mg(II) binding because a Mg(II)-coordinating water molecule is hydrogen bonded to this residue. The lack of bound Mg(II) in the structure of the D58A mutant despite the presence of 5 mM $MgCl_2$ supports this hypothesis. We attribute the residual activity observed with the D58N mutant (k_{cat} decreased 200-fold and K_m increased 5-fold compared with the wild-type enzyme) to an interaction between Asn58 and Asn124, which may occur less frequently than the Asp58−Asn124 interaction.

Relationship to Other Sequence Superfamily Members. PEP mutase is a member of an enzyme superfamily exhibiting diverse biochemical activities. PSI-Blast sequence analysis reveals that in addition to PEP mutase, the superfamily also includes carboxy-PEP mutase, P-pyr hydrolase, isocitrate lyase (ICL), 2-methyl isocitrate lyase (2MICL), a lyase of broad substrate specificity associated with carnation flower petal death (Z. Lu, Diversification of Catalytic Function Within the Isocitrate Lyase Enzyme Superfamily, Ph.D. Thesis, 2003, University of New Mexico), ketopantoate hydroxymethyltransferase (KPHMT), oxaloacetate hydrolase, and a number of homologues recently identified through genome sequencing projects. The annotations of the genome-scale sequences in databases are sometimes questionable because of the nonobvious sequence relationships between the superfamily members.

Following the structure determination of PEP mutase, structures of some other superfamily members have been reported. These include ICL in the unbound state, ICL covalently bound to pyruvic acid via the active site cysteine residue (a reaction product with bromopyruvate), the ICL complex with glyoxylic acid and succinic acid (*16*, *17*), 2MICL in the unbound state (*18*), and KPHMT with Mg(II), and with Mg(II) ketopantoate (*19*, *20*). All structures share the same α/β barrel fold with a swapped eighth helix, and a fingerprint for Mg(II) binding. PEP mutase, ICL, and 2MICL are more closely related to one another, whereas KPHMT is more diverged. It exhibits decameric association, a modified Mg(II) ligand arrangement, and differences in other key active site residues (for example, the active site PEP mutase residue, Arg159, has counterpart arginine residues in ICL

and 2MICL but not in KPHMT). The potential for conformational flexibility follows the extent of structural similarity. For ICL, it has already been documented that the same loop (connecting β4 and α4 of the α/β barrel) contains a lysine equivalent to Lys120 of PEP mutase (Lys189 in ICL from *Mycobacterium tuberculosis*). As with PEP mutase, the loop is open in the unbound state and closed when substrate analogues bind. For 2MICL, the apo structure shows the loop in an open conformation. We have recently determined the structure of 2MICL in the presence of an inhibitor, revealing the same conformational transition as seen in PEP mutase and ICL (unpublished results).

The topologically equivalent loop in KPHMT is short and cannot adopt an alternative conformation. However, the loop connecting the ensuing β/α motif (β5 and α5 of the barrel) is longer. It flanks the top of the barrel, contains a number of conserved residues, and could potentially be used as a lid. This loop is disordered in the structure of the Mg(II)-bound enzyme from *M. tuberculosis* (*19*), and is ordered in the structure of the enzyme from *E. coli*, which was determined in the presence of Mg(II) and ketopantoate product (*20*). With bound ketopantoate, the ordered loop flanks the side of the barrel and does not block access to the active site. It remains to be determined whether the loop adopts a different conformation in the presence of the substrate molecules that shields them from bulk solvent.

In conclusion, the crystal structures reported here provide new evidence that members of the PEP mutase/ICL family not only share sequence homology and overall fold but also use similar modes of flexibility, first to enable the substrate to diffuse into the active site, next to restrict the substrate during the chemical reaction, and finally to allow the product to diffuse out of the active site.

REFERENCES

1. Bowman, E. D., McQueney, M. S., Barry, R. J., and Dunaway-Mariano, D. (1988) Catalysis and thermodynamics of the phosphoenolpyruvate/phosphonopyruvate rearrangement. Entry into the phosphate class of naturally occurring organophosphorous compounds, *J. Am. Chem. Soc. 110*, 5575−5576.
2. Seidel, H. M., Freeman, S., Seto, H., and Knowles, J. R. (1988) Phosphonate biosynthesis: isolation of the enzyme responsible for the formation of a carbon−phosphorus bond, *Nature 335*, 457−458.
3. Seto, H., and Kuzuyama, T. (1999) Bioactive natural products with carbon−phosphorus bonds and their biosynthesis, *Nat. Prod. Rep. 16*, 589−596.
4. Huang, K., Li, Z., Jia, Y., Dunaway-Mariano, D., and Herzberg, O. (1999) Helix swapping between two α/β barrels: crystal structure of phosphoenolpyruvate mutase with bound Mg^{2+}-oxalate, *Struct. Folding Des. 7*, 539−548.
5. Liu, S., Lu, Z., Jia, Y., Dunaway-Mariano, D., and Herzberg, O. (2002) Dissociative phosphoryl transfer in PEP mutase catalysis: structure of the enzyme/sulfopyruvate complex and kinetic properties of mutants, *Biochemistry 41*, 10270−10276.
6. Jia, Y., Lu, Z., Huang, K., Herzberg, O., and Dunaway-Mariano, D. (1999) Insight into the mechanism of phosphoenolpyruvate mutase catalysis derived from site-directed mutagenesis studies of active site residues, *Biochemistry 38*, 14165−14173.
7. Bowman, E. D., McQueney, M. S., Scholten, J. D., and Dunaway-Mariano, D. (1990) Purification and characterization of the *Tetrahymena pyriformis* P−C bond forming enzyme phosphoenolpyruvate phosphomutase, *Biochemistry 29*, 7059−7063.
8. Otwinowski, Z., and Minor, W. (1997) Processing of X-ray diffraction data collected in oscillation mode, *Methods Enzymol. 276*, 307−326.
9. Navaza, J. (2001) Implementation of molecular replacement in AMoRe, *Acta Crystallogr. D57*, 1367−1372.
10. Brünger, A. T., Adams, P. D., Clore, G. M., DeLano, W. L., Gros, P., Grosse-Kunstleve, R. W., Jiang, J. S., Kuszewski, J., Nilges, M., Pannu, N. S., Read, R. J., Rice, L. M., Simonson, T., and Warren, G. L. (1998) Crystallography & NMR system: A new software suite for macromolecular structure determination, *Acta Crystallogr. D54*, 905−921.
11. Brünger, A. T. (1992) The free R: a novel statistical quantity for assessing the accuracy of crystal structures, *Nature 355*, 472−474.
12. Jones, T. A., Zou, J. Y., Cowan, S. W., and Kjeldgaard, M. (1991) Improved methods for building protein models in electron density maps and the location of errors in these models, *Acta Crystallogr. A47*, 110−119.
13. Anderson, V. E., Weiss, P. M., and Cleland, W. W. (1984) Reaction intermediate analogues for enolase, *Biochemistry 23*, 2779−2786.
14. Cleland, W. W. (1979) Statistical analysis of enzyme kinetic data, *Methods Enzymol. 63*, 103−138.
15. Bradford, M. M. (1976) A rapid and sensitive method for the quantitation of microgram quantities of protein utilizing the principle of protein-dye binding, *Anal. Biochem. 72*, 248−254.
16. Britton, K., Langridge, S., Baker, P. J., Weeradechapon, K., Sedelnikova, S. E., De Lucas, J. R., Rice, D. W., and Turner, G. (2000) The crystal structure and active site location of isocitrate lyase from the fungus *Aspergillus nidulans*, *Struct. Folding Des. 8*, 349−362.
17. Sharma, V., Sharma, S., Hoener zu Bentrup, K., McKinney, J. D., Russell, D. G., Jacobs, W. R., Jr., and Sacchettini, J. C. (2000) Structure of isocitrate lyase, a persistence factor of *Mycobacterium tuberculosis*, *Nat. Struct. Biol. 7*, 663−668.
18. Grimm, C., Evers, A., Brock, M., Maerker, C., Klebe, G., Buckel, W., and Reuter, K. (2003) Crystal structure of 2-methylisocitrate lyase (PrpB) from *Escherichia coli* and modelling of its ligand bound active centre, *J. Mol. Biol. 328*, 609−621.
19. Chaudhuri, B. N., Sawaya, M. R., Kim, C. Y., Waldo, G. S., Park, M. S., Terwilliger, T. C., and Yeates, T. O. (2003) The crystal structure of the first enzyme in the pantothenate biosynthetic pathway, ketopantoate hydroxymethyltransferase, from *M tuberculosis*, *Structure 11*, 753−764.
20. von Delft, F., Inoue, T., Saldanha, S. A., Ottenhof, H. H., Schmitzberger, F., Birch, L. M., Dhanaraj, V., Witty, M., Smith, A. G., Blundell, T. L., and Abell, C. (2003) Structure of *E. coli* ketopantoate hydroxymethyl transferase complexed with ketopantoate and Mg^{2+}, solved by locating 160 selenomethionine sites, *Structure 11*, 985−996.

BI036255H